INT. J. REMOTE SENSING, 1999, VOL. 20, NO. 10, 2091–2110

Narrowband to broadband conversion of Landsat TM glacier albedos

W. H. KNAP†, C. H. REIJMER and J. OERLEMANS

Institute for Marine and Atmospheric Research Utrecht, Utrecht University, P. O. Box 80.005, 3508 TA Utrecht, The Netherlands;
e-mail: W.Knap@fys.ruu.nl
† Present affiliation: Royal Netherlands Meteorological Institute, P. O. Box 201, 3730 AE De Bilt, The Netherlands; e-mail: knap@knmi.nl

(*Received 17 July 1997; in final form 5 March 1998*)

Abstract. In this paper we present an empirical relationship between the broadband glacier albedo (α) and the narrowband glacier albedos in Landsat TM bands 2 and 4 (α_2 and α_4, respectively). The relationship was established on the basis of multiple linear regression analysis of 112 ground-based simultaneous measurements of α, α_2 and α_4 made at 32 sites on the tongue of the Morteratschgletscher, Switzerland. The measurements were carried out over a representative set of glacier surface types ranging from completely debris-covered glacier ice ($\alpha = 0.08$) to dry snow ($\alpha = 0.86$). The regression model explains more than 99% of the variance of the broadband albedo and the root-mean-square value of the residuals is only 0.009. The relationship enables users of Landsat TM data to make an accurate estimate of the broadband albedo on the basis of narrowband albedos without having to classify the glacier surface.

1. Introduction

Since the Little Ice Age ended in the middle of the nineteenth century most glaciers on Earth have been shrinking dramatically. According to a recent estimate the total surface ice mass in the European Alps was reduced by about 50% during the period 1850–1975 (Haeberli 1995). Worldwide glacier retreat provides one of the clearest signals of a changing global climate. To understand how glaciers respond to a changing climate it is essential to have knowledge of the surface energy-balance of glaciers. On mid-latitude valley glaciers most of the energy for melting is provided by absorption of solar radiation and by turbulent exchange of sensible heat. Since solar radiation provides typically 50–75% of the melt energy it is important to find suitable expressions for the albedo which can be used in models that simulate glacier melt. Such expressions are often derived from field measurements carried out at just a few sites on the glacier surface (e.g. Oerlemans 1993). However, one needs a very large number of spatially distributed measurements in order to describe the variation in the albedo over the whole glacier surface. As far as we know albedo measurements of this kind have been carried out only on the Haut Glacier d'Arolla, a small valley glacier in the Swiss Alps (Arnold *et al.* 1996, Brock 1997, Knap *et al.* 1998).

Making measurements on glaciers requires considerable effort. Often the glaciers are not easily accessible and high melt rates cause a continuously changing surface

International Journal of Remote Sensing
ISSN 0143-1161 print/ISSN 1366-5901 online
http://www.tandf.co.uk/JNLS/res.htm
http://www.taylorandfrancis.com/JNLS/res.htm

relief during the ablation season. In winter snow-covered crevasses make the glacier even less accessible and avalanches may threaten lives and destroy instruments. This explains why glacier-wide albedo measurements are so scarce. Satellite remote sensing has the potential to overcome the specific problems associated with ground measurements. Operational satellites like Landsat and NOAA provide complete coverage of glaciers and ice sheets (see e.g. Williams and Ferrigno 1995, Knap and Oerlemans 1996). It is improbable that such coverage will ever be achieved by ground-based measurements.

The deriving of glacier surface albedo from satellite measurements is not simple. For example information is required to correct for the intervening atmosphere and for anisotropic reflection of the glacier surface. Optical radiometers on board the Landsat and NOAA satellites (Thematic Mapper (TM) and Advanced Very High Resolution Radiometer (AVHRR), respectively) have been designed to operate in distinct wavelength bands (typical band width: 60–380 nm). The band structure has been chosen to exploit spectral differences in the albedo of different types of surfaces. However, for energy-balance applications one needs to know the broadband or total albedos (i.e. covering the entire solar spectrum) rather than the narrowband albedos (i.e. covering wavelength intervals as mentioned above). Because the glacier albedo generally depends strongly on wavelength as well as on the physical composition of the surface (figure 1) there is no obvious way of deriving the broadband albedo from narrowband albedo measurements. This can be regarded as a major problem in the retrieval of surface albedo from satellite measurements.

In order to find a suitable expression for narrowband-to-broadband conversion of TM glacier albedos we approached the problem empirically by carrying out simultaneous measurements of narrowband (TM 2 and 4) and broadband albedos over a representative set of glacier-ice and snow surfaces. The measurements were carried out on the Morteratschgletscher (Vadret da Morteratsch) during the periods April–September 1996 and February–April 1997. This relatively large valley glacier is situated in eastern Switzerland in the Bernina mountain range (figure 2). The present-day length of the glacier is 7.0 km and it extends from over 4000 m (Piz

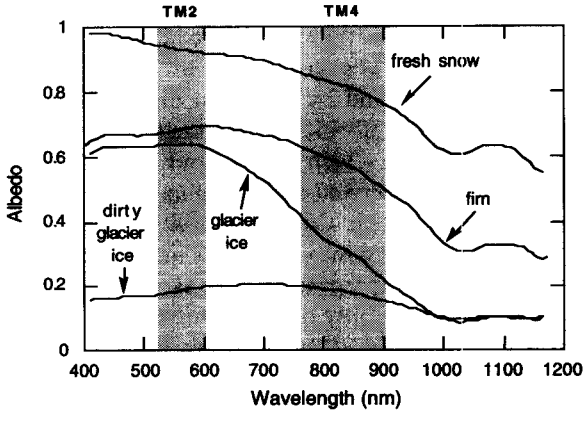

Figure 1. Typical curves of spectral glacier albedo. Two wavelength bands of the Landsat Thematic Mapper are indicated. TM2 operates in the visible wavelengths (520–600 nm) and TM4 in the near-infrared wavelengths (760–900 nm). Figure modified from Zeng *et al.* (1984) cited in Hall *et al.* (1988).

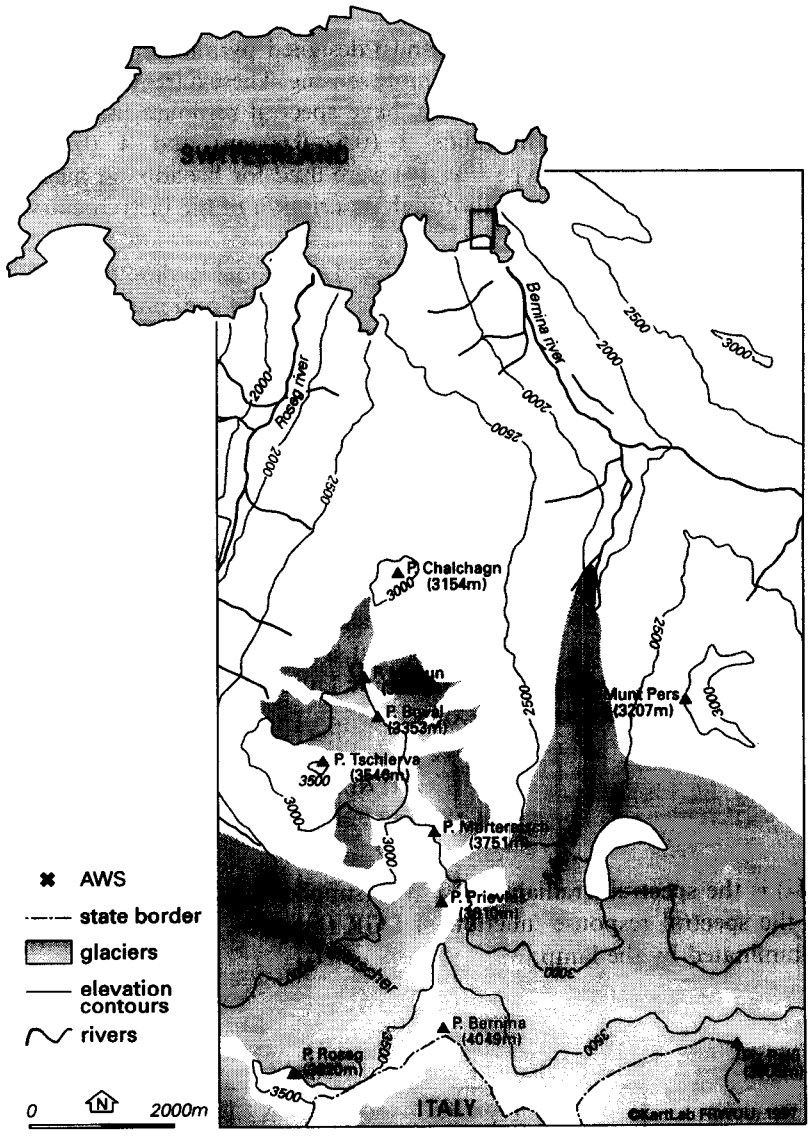

Figure 2. Map showing the Morteratschgletscher and the Automatic Weather Station (AWS).

Bernina) to about 2050 m (glacier front). Since about AD 1850 the glacier has retreated over a distance of 1.9 km, which makes it a classic example of glacier recession (Maisch *et al.* 1993).

The measurements over snow were carried out near an Automatic Weather Station (AWS) that is permanently situated on the tongue of the Morteratschgletscher at an elevation of 2100 m. The AWS has been installed there to provide a multi-annual data set on basic meteorological quantities in the ablation zone of a valley glacier (Oerlemans 1997). In order to cover the entire range of glacier ice albedo values numerous measurements were carried out within an area of about 300–100 m^2 in the surroundings of the AWS (figure 2).

2. Instruments and calibration

Kipp & Zonen (Delft, The Netherlands) designed pyranometers specifically for measurements related to Landsat TM remote sensing. These narrowband pyranometers, one facing up and one facing down, have spectral response functions close to the nominal TM wavelength bands 2 (0.52–0.60 μm) and 4 (0.76–0.90 μm). Conventional pyranometers (type CM 14) were used for broadband measurements (0.3–3.0 μm). Knap (1997) gives a thorough description of the instruments and their specifications.

The narrowband pyranometers, named Landsat Global Radiometer (LGR), were built on the basis of a modification of CUVA1 ultraviolet radiometers. Basically the LGRs consist of a silicon photodiode, several filters, a diffuser and a glass dome. Instrument response functions of LGR and TM are presented in figure 3. As can be seen from this figure, the LGR response functions are shifted by about 10 nm relative to the TM response functions. Note that the LGR response functions are closer to the nominal TM values than are the actual TM response functions. Because the albedo is a slowly changing function of wavelength (see figure 1) the wavelength shift is not very important and causes only small errors ($\ll 0.01$ in albedo).

All instruments were calibrated carefully at the calibration laboratory of the Royal Netherlands Meteorological Institute (KNMI, De Bilt) before and after the field measurements. The broadband pyranometers were calibrated against a CM 11 standard. The LGRs were calibrated against a 1000 W quartz–halogen tungsten coiled-coil filament lamp (type F-359, Optronic Laboratories). Calibration factors K ($\mathrm{W\,m^{-2}\,mV^{-1}}$) were obtained as follows:

$$\mathrm{K} = \frac{\int_0^\infty I(\lambda)\, R(\lambda)\, \mathrm{d}\lambda}{S} \tag{1}$$

Here $I(\lambda)$ is the spectral irradiance of F-359 (supplied by Optronic Laboraties) and $R(\lambda)$ is the spectral response function of LGR (figure 3). S is the signal in mV of LGR illuminated by the lamp.

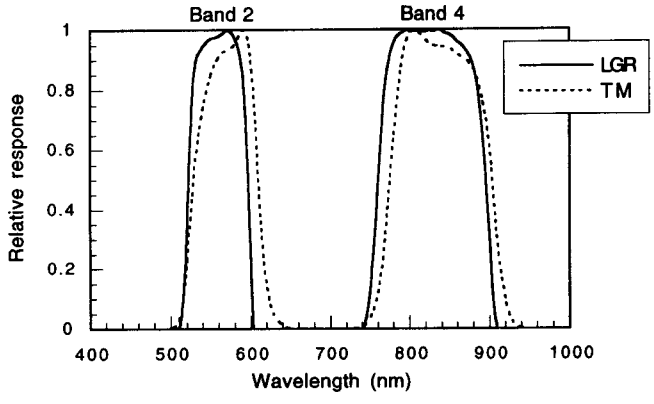

Figure 3. Spectral response functions of the Landsat Global Radiometers (LGR) and of Landsat-5 Thematic Mapper (TM) bands 2 and 4 (nominal wavelength bands: 520–600 nm and 760–900 nm).

To gain insight into the general performance of the LGRs we carried out comparative measurements with a spectroradiometer of KNMI at a test site over a period of several days in June 1995. The details of these measurements can be found in Knap (1997). It appeared that the LGR irradiances agreed very well with the irradiances measured by the spectrometer, which inspired confidence in the LGRs. It is estimated that the error in narrowband irradiances is less than 3% during typical measurement conditions (little cloudiness, solar zenith angle $< 60°$). According to the CM 14 specifications the uncertainty in broadband irradiance is of the order of 2%.

The measurements on the glacier were performed using a construction consisting of a horizontal aluminium rod (3.5 m length) supported by two tripods (see Knap, 1997). The three pairs of up and down facing pyranometers were attached to the middle of the rod. Sampling (every 10 s) and storage (2 min mean values) of the data were performed by means of a Campbell CR 10 datalogger. Power was supplied by lithium batteries.

3. Narrowband and broadband global radiation

Before proceeding to albedo measurements we give a typical example of measured global radiation on the Morteratschgletscher during a clear-sky day (20 April 1996) (figure 4). At solar noon the narrowband TM 2 and 4 pyranometers receive typically 11–12% of the broadband global radiation. In the morning and afternoon abrupt changes in the irradiance indicate the presence of the surrounding mountains which cast shadows over the instruments. By the end of April shading angles are 33° in the east and 23° in the west. The reduction in daily mean global radiation appears to be 16%, which is considerable for the time of year.

Comparative measurements with an accurate standard could obviously not be accomplished in the field. However, a rough idea about the correctness of the measurements was obtained by simulating narrowband and broadband irradiances with a radiative transfer model. The model used is based on the 24-band radiation scheme presented by Slingo and Schrecker (1982). The scheme uses the δ-Eddington multiple scattering method and treats Rayleigh scattering and absorption by

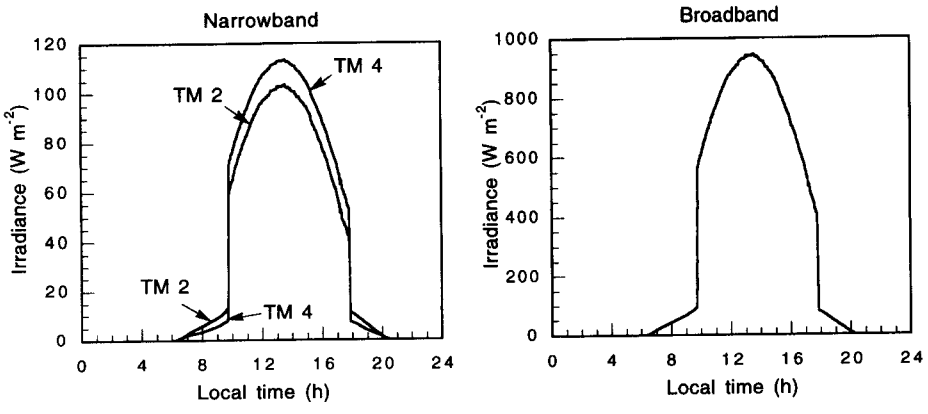

Figure 4. Two-minute mean measurements of narrowband (TM 2 and 4) and broadband global radiation on the Morteratschgletscher (AWS site) during a cloudless day (20 April 1996). At solar noon the solar zenith angle is 34.7°.

water vapour and ozone. Aerosols were not included. For convenience we define the effective transmissivity of the atmosphere τ_{eff} by relating the global irradiance (narrowband or broadband) at the surface (I_s) to the irradiance outside the earth's atmosphere (I_0):

$$I_s = \tau_{eff} I_0 \cos\theta_0 \tag{2}$$

Here θ_0 is the solar zenith angle. In the case of a cloudless atmosphere τ_{eff} is determined largely by absorption of ozone, water vapour, aerosols and Rayleigh scattering effects of air molecules. Absorption due to ozone has a relatively strong influence on the transmissivity in TM 2, whereas water vapour is the main absorber in TM 4.

Measured and modelled values of τ_{eff} at solar noon on 20 April 1996 are shown in table 1. Considering the atmospheric conditions during the measurements (clear sky) and the elevation of the measurement site (2100 m a.s.l.), it is not surprising that the values suggest a highly transparent atmosphere. The narrowband transmissivities are higher than the broadband transmissivity; this is due to the fact that the bands are situated at wavelengths that are not within the absorption bands of the major constituents of the atmosphere and are beyond wavelengths where Rayleigh scattering is important. The good agreement between measured and modelled values of τ_{eff} gives us confidence in the accuracy of the irradiance measurements carried out at the glacier surface.

4. Evolution of the surface albedo

Daily values of the narrowband albedos α_2 and α_4 and the broadband albedo α measured at the AWS site (figure 2) are shown in figure 5(*a*) and (*b*). Each value represents the ratio of daily mean upward to downward irradiance. In the following we will give a description of the evolution of the albedo during the ablation season of 1996 (figure 5(*a*)) and during the transition from winter to spring in 1997 (figure 5(*b*)).

At the beginning of the first period (around 18 April 1996) about 45 cm of snow covered the ice surface, which explains the high albedo values. On 3 May a snowfall of at least 25 cm temporarily covered the glass domes of the pyranometers so that reliable data were not available on 3 and 4 May. The snowfall was followed by a relatively warm and sunny spell so that on 15 May glacier ice became exposed at the surface ($\alpha < 0.4$). Subsequently two snowfalls increased the albedo again. The first half of June was characterized by fair and sunny weather and the albedo was reduced to values < 0.3. After a period of variable weather a significant change in conditions occurred on 21/22 June with the arrival of a frontal system. The

Table 1. Global radiation at solar noon ($\theta_0 = 34.7°$) on 20 April, 1996. The extraterrestrial values ($I_0 \cos\theta_0$) were derived from Iqbal (1983), whereas the values at the glacier surface (I_s) were measured directly (see figure 4). The transmissivity (τ) is the ratio $I_s / I_0 \cos\theta_0$ (see equation (2)).

Spectral range	$I_0 \cos\theta_0$ (W m^{-2})	I_s (W m^{-2})	τ^a	τ^b
TM 2	108	103	0.96	0.96
TM 4	114	113	0.99	0.95
Broadband	1113	946	0.85	0.85

[a] Derived from measurements. [b] Derived from a radiative transfer model (see text).

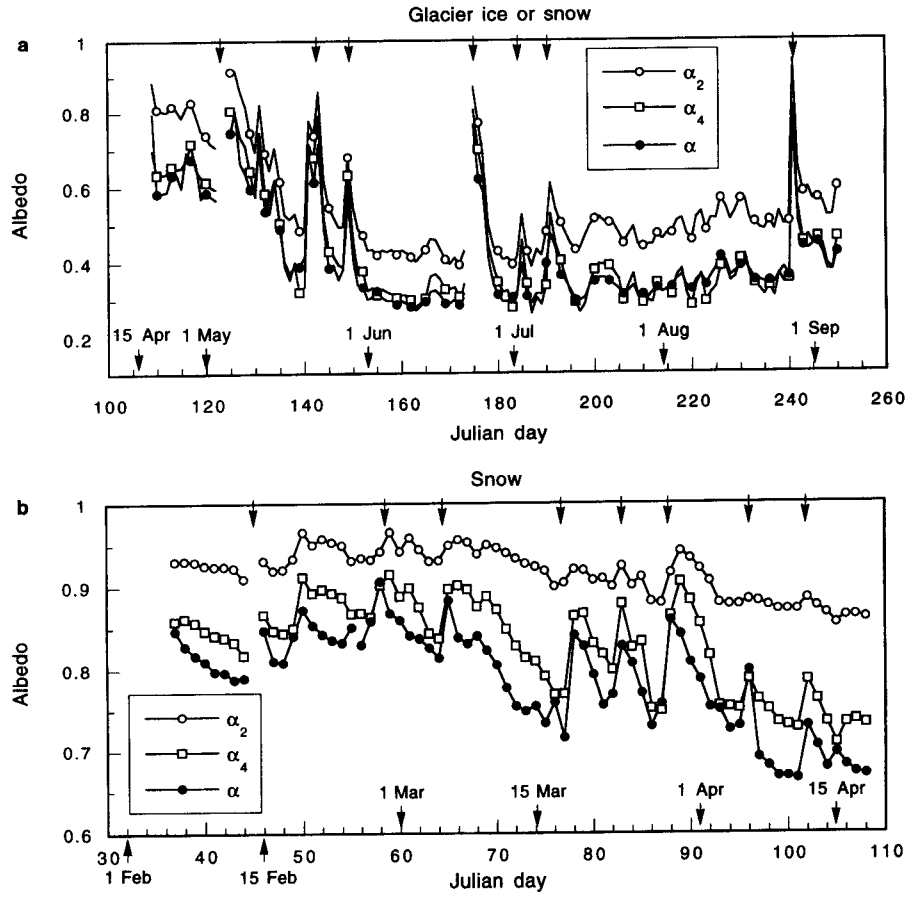

Figure 5. Narrowband (α_2: TM 2, α_4: TM 4) and broadband (α) daily albedo at the AWS site for the period (*a*) 18 April–6 September 1996, and (*b*) 6 February–18 April 1997. Daily albedo values were calculated on the basis of daily mean irradiances. Gaps in the data indicate periods during which the pyranometers were covered by snow. The arrows at the top of the figures indicate major snowfalls. Note the scale difference between the two figures.

temperature dropped, severe thunderstorms developed and fresh snow fell on the glacier. Consequently the albedo increased to values between 0.7 and 0.8. Within a few days the snow melted away and the albedo decreased again to values around 0.3. There were no major snowfalls at the AWS site until 27 August and the albedo was consequently less variable than in spring and early summer. Nevertheless a slight increase can be observed, which may be related to occasional snow showers. It seems that these increase the albedo even if the snow has melted away.

The second series of albedo measurements was carried out over a relatively deep snowpack (figure 5(*b*)). Snowpack thickness varied between 90 and 115 cm, which is certainly enough to obliterate the effect of the underlying ice surface on the albedo (see e.g. Wiscombe and Warren 1980, Oerlemans and Knap 1998). Initially the snowpack was dry and the albedo was high (0.85). However, due to mild weather with maximum air temperatures between 2° and 5° C, some melting took place and during the first week of the measurement period the albedo decreased gradually to

values below 0.8. Visual evidence for the fact that melting took place was provided particularly by the development of melt cups. The first snowfall occurred on 13/14 February during strong westerly winds. Consequently the albedo increased again up to values that are typical for freshly fallen snow. Subsequently the albedo decreased under the influence of metamorphosis. This pattern of increasing and decreasing albedos occurred frequently during the entire measurement period. The pattern appears to be superimposed on a decreasing trend which reflects overall metamorphosis of the snowpack. Eventually the albedo reached values around 0.67.

All measurements of α_2 (TM 2) and α_4 (TM 4) presented in figures 5(*a*) and (*b*) show that the albedo in the near-infrared is lower than in the visible. This result is consistent with the spectral albedo curves of fresh snow, firn and glacier ice presented by Zeng *et al.* (1984) (figure 1). The broadband albedo of glacier ice (figure 5(*a*), lowest albedo values) is generally close to the near-infrared albedo, which implies that high albedo values in the visible are to a large extent compensated by low albedo values in the infrared. It should be noted that the AWS site where the measurements were carried out was situated on a relatively clean part of the glacier. Spatially distributed measurements over the glacier tongue showed that, closer to the margin of the glacier, the albedo was frequently lower and the difference between visible and near-infrared albedo was less pronounced (see also §5.1).

In common with previous studies (e.g. Warren 1982, Grenfell and Mullen 1994) the measurements carried out over snow (figure 5(*b*)) show that the albedo is generally high in the visible but drops off steeply in the near-infrared. Apparently the contrast between shorter and longer wavelengths is so large that in general $\alpha < \alpha_4$. Furthermore the measurements reveal that reductions in the albedo in the visible are usually smaller than reductions in the near-infrared. As an example we focus on the period 7–16 March (Julian days 66–75). During these spring-like days there was no precipitation and temperatures were mild (0° C level frequently around 3000 m a.s.l., which is well above the AWS site). These conditions led to significant densification of the snowpack. The visible albedo α_2 decreased from 0.96 to 0.92, whereas α_4 dropped from 0.90 to 0.79. The reduction in the total albedo is of the same order of magnitude as the reduction in the near-infrared albedo (*ca* 0.11). Therefore a decrease in the broadband albedo is primarily due to a decrease in the near-infrared. Again this result is in agreement with what is usually found in literature.

5. Narrowband to broadband conversion

In order to derive accurate empirical relationships, sets of 62 (for glacier ice), 50 (for snow) and 112 (for glacier ice and snow) data points were fitted to the following model:

$$\alpha = a\alpha_2 + b\alpha_2^2 + c\alpha_4 + d\alpha_4^2 \tag{3}$$

The model has no obvious physical basis and was chosen simply because it proved capable of predicting the broadband albedo with high accuracy. Constants were not allowed so that the following condition was satisfied: if $\alpha_2 \to 0$ and $\alpha_4 \to 0$ then $\alpha \to 0$. The coefficients *a*, *b*, *c* and *d* were obtained by multiple linear regression analysis. Reduced models (one or more coefficients equal to 0) will be presented if these give equally accurate results as the full model. To indicate how well the model agrees with the data we will give values of the linear correlation coefficient (r^2) and of the root-mean-square difference of the (modelled–measured) residuals (σ_{res}) for each fit.

5.1. *Glacier ice*

In order to derive a relationship for glacier ice two series of measurements were used. The first series consists of a selection of 31 periods with little cloud cover during the interval May–August 1996. These periods, ranging from several hours to one day at most, were selected on the basis of visual inspection of the measured daily course in global radiation. Because only perfectly smooth parts were selected (such as presented in figure 4), there is a fair chance that the corresponding measurements were carried out under (almost) clear conditions. The 31 albedo values, calculated on the basis of time-averaged irradiances, are shown in figure 6. The variability is due primarily to different concentrations of ablation material and meltwater at the glacier surface.

As was mentioned before, the AWS site where the above-mentioned measurements were carried out was situated on a relatively clean part of the glacier. Consequently the albedo was high. In order to cover the entire range of ice albedo values an extensive survey of the glacier tongue was made during the second week of September 1996. During fair weather 31 sites were visited and at these sites narrowband and broadband albedo measurements were carried out. Virtually all surface types were encountered; from completely debris-covered ice on the eastern lateral moraine to clean and bright ice in the surroundings of the AWS. Most of the time the sky was cloudless, although some measurements were made when cumulus was present (always less than 3 octas). During none of the measurements did these clouds cause shading and direct radiation was always dominant. The measurements are therefore representative of typical conditions during which Landsat data, suitable for deriving the surface albedo, are acquired.

The albedo values as measured at the 31 sites are presented in figure 7. Each column represents an average of 10 surface-parallel readings made during a period of 1.5 min. For convenience the data set has been divided into three groups corresponding to measurements over dirty ice (group 1), fairly clean ice (group 2) and clean ice (group 3). We emphasise that this is not a strict separation: there is rather a smooth transition from one group to the next. Group 1 measurements were carried out over ice surfaces partly or entirely covered by fine-grained material like sand, silt or clay and/or by coarser material like pebbles. Reading 21 was taken on the

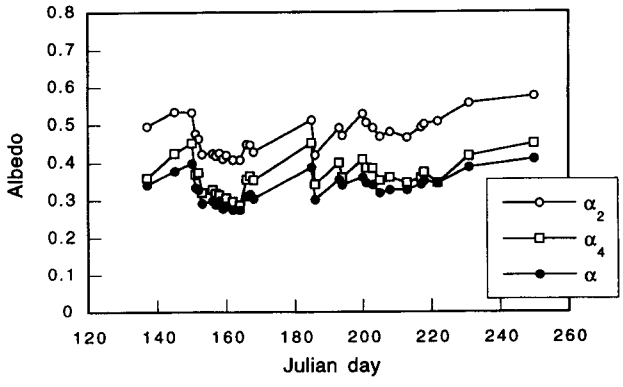

Figure 6. Measurements of α_2 (TM 2), α_4 (TM 4) and α (broadband) carried out at the AWS site during the period May–August 1996. Each data point refers to a period (several hours or a day at most) during which there was little to no cloud cover.

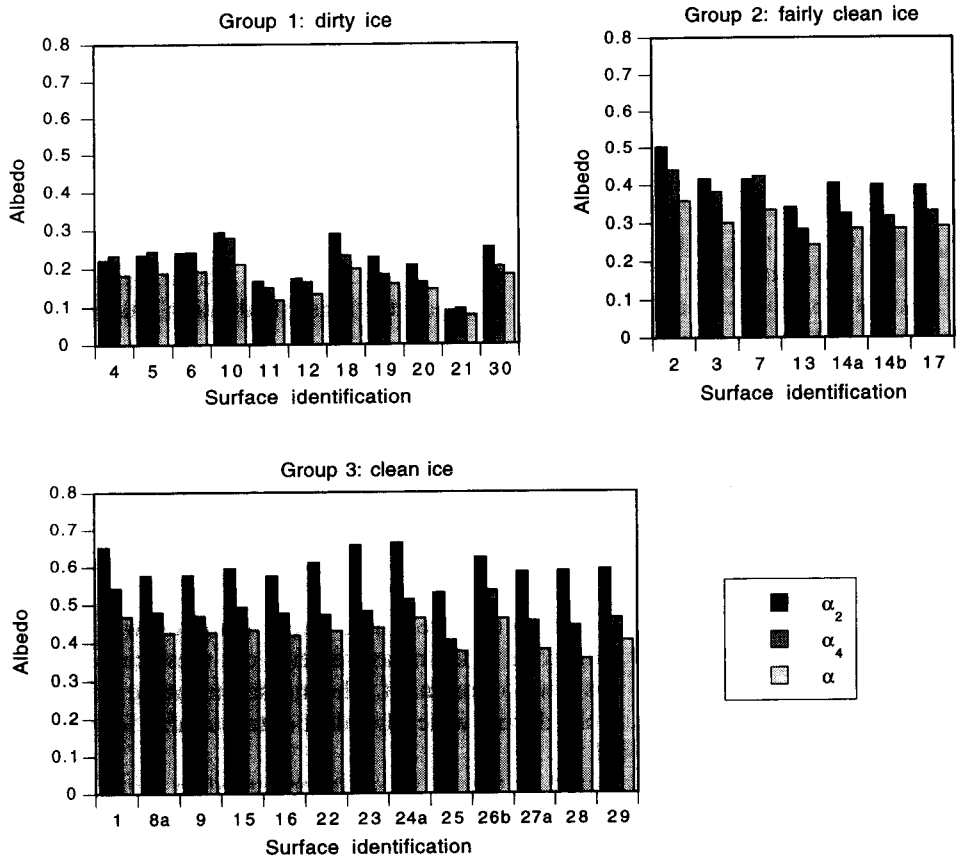

Figure 7. Measurements of α_2 (TM 2), α_4 (TM 4) and α (broadband) carried out at 31 sites on the tongue of Morteratschgletscher during the period 7–12 September, 1996. The dataset is divided into three groups corresponding to measurements over dirty ice (group 1), fairly clean ice (group 2) and clean ice (group 3).

eastern lateral moraine where the ice surface is buried under a thick layer of rock debris. Measurements collected in group 2 were carried out at sites where the ice surface is partly covered by fine-grained material only. Measurements carried out over clean ice with a low concentration of ablation material at the surface were brought together in group 3. This type of ice was found particularly in the middle of the glacier, for example near the AWS, and looked very bright to the human eye. This is not surprising considering the magnitude of the albedo in the visible band ($\alpha_2 = 0.53$–0.66). Due to aggregates of coarse ice-crystals, some of which measured several centimetres in diameter, clean-ice surfaces were often rough. Most fine-grained material appeared to be collected in cryoconite holes. Probably due to the high albedo little meltwater was present on clean ice. Dirty ice was usually much wetter than clean ice.

On the basis of the measurements carried out at the AWS site (figure 6) and at the different sites on the glacier (figure 7) the following fit was found (using 62 data points):

$$\alpha = 0.427\alpha_2 + 0.354\alpha_1 \tag{4}$$

The linear correlation coefficient is high ($r^2 = 0.995$) and the rms value of the residuals is low ($\sigma_{res} = 0.007$), which indicates that the model agrees very well with the measurements. The quality of the fit is visualized in figure 8 where the modelled albedo is plotted against the measured albedo. It is clear that equation (4) applies very well to all data and there is no point in deriving relationships for every type of glacier ice (further discussion is to be found in §5.4).

5.2. *Snow*

In order to derive a relationship that is applicable to new snow (fine grains), spring or old snow (course grains) and snow packs of different thickness, two series of measurements were carried out at the AWS site. The first series consists of 25 clear-sky measurements made between 19 April and 24 June, 1996 (figure 9, upper panel). Clear-sky periods were selected in the same way as described in §5.1. Most measurements (19) were made over shallow snow packs (1–5 cm) shortly after snow falls in spring or early summer. The underlying ice surface very probably had some effect on the albedo. The remaining six measurements were taken over deeper snow packs (17–43 cm) just before the ice surface of 1995 became exposed at the surface. The second series of clear-sky measurements was carried out over deep snow packs (90–115 cm) during the period 6 February–18 April, 1997 (figure 9, lower panel). Surface conditions ranged between dry fine-grained snow and wet course-grained snow. Although snow fell regularly on the glacier (see figure 5(*b*)) the period was characterized by extremely fair weather. As many as 25 more or less cloud-free days could be selected. To avoid instrumental errors as a result of deviations from the cosine law, only data acquired around solar noon were used to calculate albedo values.

On the basis of multiple linear regression to the 50 data points the following best fit was derived:

$$\alpha = 0.251\alpha_2 + 0.435\alpha_4 + 0.238\alpha_4^2 \tag{5a}$$

As for the glacier ice relationship (equation (4)) the linear correlation coefficient is high ($r^2 = 0.991$) and the rms value of the residuals is low ($\sigma_{res} = 0.010$), so the model agrees well with the measurements. For a fully linear model the results are slightly

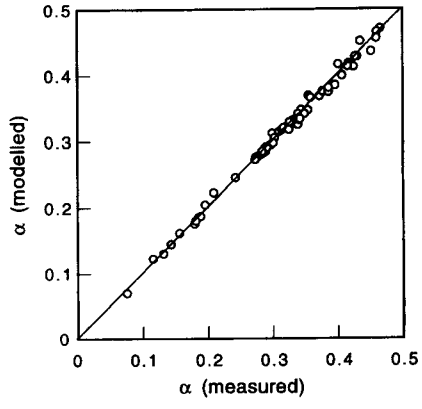

Figure 8. Modelled broadband albedo *versus* measured broadband albedo of glacier ice. The modelled albedo was calculated on the basis of the regression model given by equation (4) and the narrowband albedo measurements in TM bands 2 and 4.

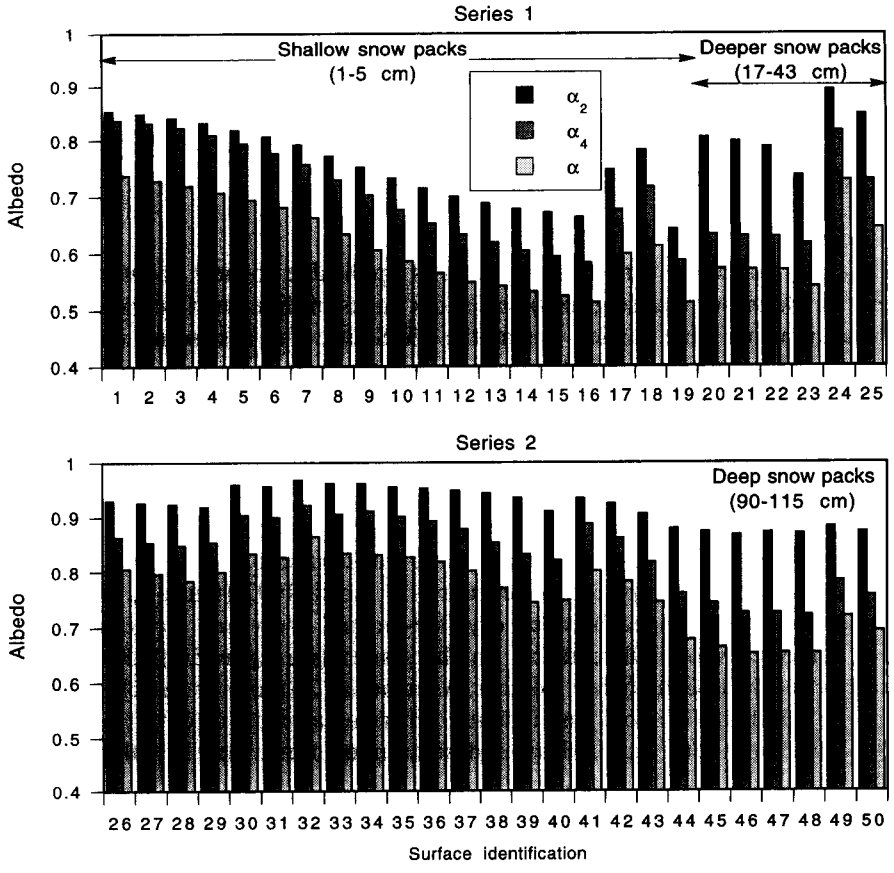

Figure 9. Measurements of α_2 (TM 2), α_4 (TM 4) and α (broadband) carried out at the AWS site during the period 19 April–24 June 1996 (series 1) and 6 February–18 April 1997 (series 2). All measurements were carried out over snow during clear-sky conditions.

less perfect: $r^2 = 0.972$ and $\sigma_{res} = 0.018$. A model quadratic in α_2 and linear in α_4 gives similar results to equation (5a). Neither alternative fit is given here. Again we visualize the performance of the fit by plotting modelled albedo values against measured albedo values (figure 10). The figure demonstrates convincingly that a single relationship applies to both fine-grained and coarse-grained snow and to snow packs of various thickness.

Since TM band 2 (visible radiation) frequently saturates over snow we also derived an expression that is only a function of TM band 4 (near-infrared radiation):

$$\alpha = 0.782\alpha_4 + 0.148\alpha_4^2 \tag{5b}$$

Although not performing as well as equation (5a) this single-band model agrees fairly well with the measurements ($r^2 = 0.983$ and $\sigma_{res} = 0.014$) and allows an accurate calculation of the albedo in cases where TM band 2 is saturated.

5.3. *Glacier ice and snow*

Since it is not easy to distinguish objectively between ice and snow surfaces in satellite imagery it is extremely useful to have one model that applies to any glacier

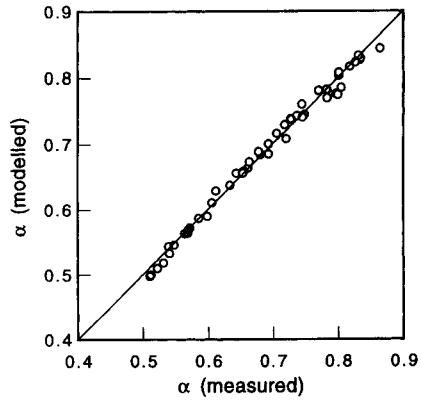

Figure 10. Modelled broadband albedo *versus* measured broadband albedo of snow. The modelled albedo was calculated on the basis of the regression model given by equation (5a) and the narrowband albedo measurements in TM bands 2 and 4. The measurements were carried out over fine-grained and coarse-grained snow and over snow packs of various thickness.

surface, whether it be glacier ice or snow. Therefore all data points (112) were subjected to linear regression analysis. The best fit appeared to be as follows:

$$\alpha = 0.726\alpha_2 - 0.322\alpha_2^2 - 0.051\alpha_4 + 0.581\alpha_4^2 \tag{6}$$

The linear correlation coefficient is high ($r^2 = 0.998$) and the rms value of the 112 residuals is small ($\sigma_{res} = 0.009$). The fit is excellent (figure 11) and it is clear that *this empirical relationship can be used without having to make any classification of the glacier surface.*

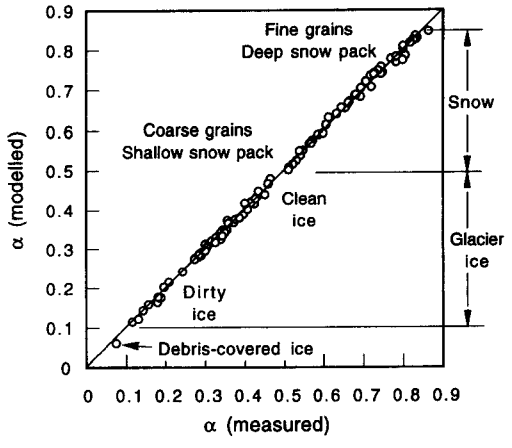

Figure 11. Modelled broadband albedo versus measured broadband albedo of glacier ice and snow. The modelled albedo was calculated on the basis of the regression model given by equation (6) and the narrowband albedo measurements in TM bands 2 and 4. Different glacier surface types are indicated.

5.4. *Verification of existing weighting functions*

5.4.1. *Background*

Existing relationships for estimating the broadband albedo from narrowband TM albedos are based upon the assumption that a spectral albedo curve can be approximated by wavelength intervals $\Delta\lambda_i$ of uniform albedo α_i, i.e.

$$\alpha = \frac{\sum_i \alpha_i \int_{\Delta\lambda_i} F\downarrow(\lambda)\,d\lambda}{\int F\downarrow(\lambda)\,d\lambda} \tag{7}$$

Here, α is the broadband albedo and $F\downarrow(\lambda)$ is the global spectral irradiance. It follows that the broadband albedo can be written as a linear combination of narrowband albedos:

$$\alpha = \sum_i c_i \alpha_i \tag{8}$$

Such an expression is often referred to as a *weighting function.* The coefficients c_i represent the ratio of global narrowband irradiance (in wavelength band $\Delta\lambda_i$) to broadband global irradiance. The number of terms and the values of the coefficients thus depend primarily on the choice of the wavelength bands $\Delta\lambda_i$. This choice is determined by the spectral albedo of the surface and by the wavelength location of the bands of the satellite instrument. This approach was proposed by Brest and Goward (1987) and Brest (1987) and has been applied to snow surfaces and glaciers by e.g. Duguay and LeDrew (1991, 1992), Duguay (1993) and Gratton *et al.* (1993).

Weighting functions used in the studies mentioned above are presented in table 2. Gratton *et al.* (1993) divided the solar spectrum into four intervals and calculated the coefficients c_i by means of the LOWTRAN-6 code. The intervals were chosen on the basis of generalised spectral albedo curves of ice and snow (see figure 14 and §5.4.3). Since the third interval $\Delta\lambda_3$ is not represented by any of the TM bands it is assumed that the albedo in this interval (indicated by $\alpha(\Delta\lambda_3)$) is a certain fraction of the albedo in TM band 4 (α_4). In equations (9b) and (9c) $\alpha(\Delta\lambda_3)/\alpha_4 = 0.3$, whereas in Equation (9d) $\alpha(\Delta\lambda_3)/\alpha_4 = 0.63$. This difference reflects a difference in snow grain size: for large grains the fraction is small and vice versa (Wiscombe and Warren, 1980).

To illustrate the dependency of $\alpha(\Delta\lambda_3)/\alpha_4$ on grain size we show simulated spectral albedo curves of snow for different effective grain sizes r_0 in figure 12 (based on

Table 2. Weighting functions for ice and snow presented in literature and verified by means of the narrowband and broadband albedo measurements made at the Morteratschgletscher (figure 13). The indices refer to Landsat TM bands 2 (visible), 4 (near-infrared) and 7 (mid-infrared).

Weighting function	Designed for	Equation
$\alpha = 0.493\alpha_2 + 0.507\alpha_4$	Dirty ice	(9a)[a]
$\alpha = 0.493\alpha_2 + (0.203 + 0.150 \times 0.3)\alpha_4 + 0.154\alpha_7$	Clean ice and snow	(9b)[a]
$\alpha = (0.493 \times 1.12 + 0.203 + 0.150 \times 0.3)\alpha_4 + 0.154\alpha_7$	Snow	(9c)[a]
$\alpha = 0.526\alpha_2 + (0.232 + 0.130 \times 0.63)\alpha_4 + 0.112\alpha_7$	Snow	(9d)[b]

References: [a]Gratton *et al.* (1993) and [b]Duguay and LeDrew (1992).

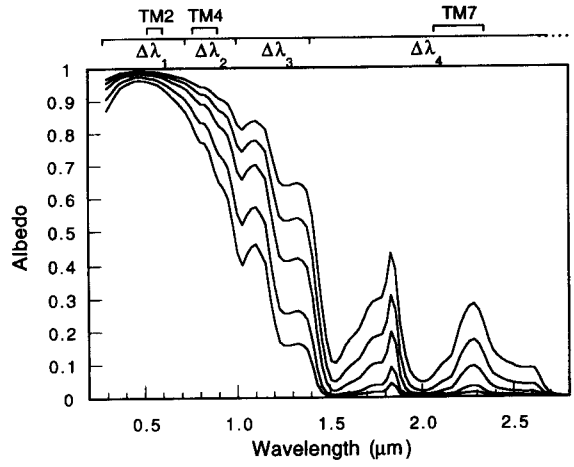

Figure 12. Spectral albedo of pure snow according to model calculations based on Mie scattering theory and on the δ-Eddington approximation (Wiscombe and Warren, 1980). Effective snow grain-sizes are 50, 100, 200, 500 and 1000 μm from top to bottom.

Wiscombe and Warren, 1980). The approximation $\alpha(\Delta\lambda_3)/\alpha_4 = 0.3$ made in equation (9c) should be valid for coarse-grained snow ($r_0 \sim 1000\,\mu$m), whereas $\alpha(\Delta\lambda_3)/\alpha_4 = 0.63$ (equation (9d)) is applicable to snow with finer grains. It should be noted that Gratton *et al.* (1993) and Duguay and LeDrew (1992) used not only different values of $\alpha(\Delta\lambda_3)/\alpha_4$, but also different values of c_i (compare equations (9c) and (9d)), although the wavelength bands $\Delta(\lambda_i)$ are the same. We have no obvious explanation for this discrepancy. Equation (9c) is used in cases where TM 2 is saturated (which occurs frequently over highly reflective surfaces like snow). In that case an additional approximation is made: $\alpha_2 = 1.12 \times \alpha_4$.

5.4.2. *Verification with Morteratsch measurements*

The measurements of narrowband and broadband albedo carried out on the Morteratschgletscher provide an opportunity to verify the weighting functions presented in table 2. Unfortunately measurements in TM band 7 were not carried out. Verification is therefore only possible if the last term in equations (9b)–(9d) is neglected. The simulations of the spectral albedo (figure 12) suggest that the error involved is not large, especially for coarse grains. For $r_0 = 50\,\mu$m we find that $0.154 \times \alpha_7 \sim 0.03$ and for $r_0 = 200\,\mu$m the term is already less than 0.01. The error is therefore only of some importance for dry powder snow (say $r_0 < 200\,\mu$m).

Weighted and measured albedo values are shown in figures 13(*a*) (glacier ice) and (*b*) (snow). The following conclusions can be drawn:

1. Weighted albedos of glacier ice calculated with equation (9a) agree poorly with measured albedos. Even if only measurements carried out over dirty ice (say $\alpha = 0.1$–0.2) are considered, the weighting function does not perform well. This is a striking result because the function was designed for calculating albedos of dirty ice. On the basis of our measurements it seems that the weighting function applies only to the lowest albedos which relate to completely debris-covered ice (figure 13(*a*), lowest data point).
2. Although designed for clean ice, equation (9b) applies to both dirty and clean

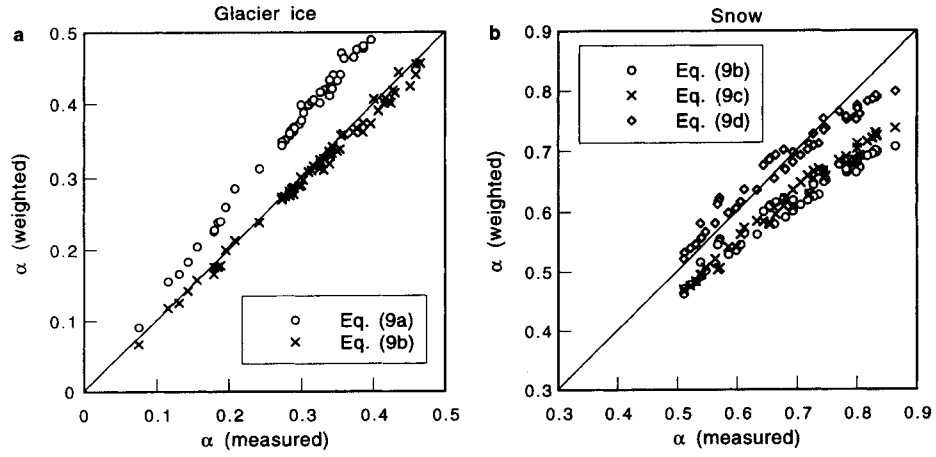

Figure 13. Weighted albedo *versus* measured albedo of glacier ice (*a*) and snow (*b*). The weighted albedo was calculated on the basis of weighting functions presented in earlier literature and enumerated in table 2.

glacier ice. The weighting function has a slight tendency to underestimate high albedos.

3. Weighted albedos of snow calculated with equations (9b) and (9c) agree poorly with measured albedos. The use of these weighting functions results in strong underestimates of the albedo. The pronounced difference between weighted and measured albedo for high albedos may be due to the neglect of α_7. However, this neglect cannot be the cause of the discrepancies for the lower albedos (say $\alpha < 0.7$) because here the corresponding grain sizes are certainly large enough for α_7 to be sufficiently small.
4. Equation (9d) gives satisfactory results, although the weighting function tends to underestimate high albedos. Since these albedos were measured over powder snow this tendency may be due to neglect of the term $0.112 \times \alpha_7$.

5.4.3. *Discussion*

As mentioned above, the formulation of existing weighting functions (table 2) is based on a division of generalized spectral albedo curves into segments of uniform albedo. The curves for dirty ice, clean ice and snow that formed the basis for equations (9a)–(9c) are shown in figure 14. Also shown are characteristic (averaged) measurements carried out on the Morteratschgletscher over deep snow, shallow snow, glacier ice (clean, fairly clean and dirty) and debris-covered glacier ice. In the following a comparison will be made between the generalized curves and our measurements and an attempt will be made to explain the results presented above.

The measurements over glacier ice show that the albedo decreases in the near-infrared (figure 14). In all cases (i.e. for clean and dirty glacier ice) the broadband albedo α is lower than α_2 and α_4, which indicates that the spectral albedo decreases still further at wavelengths beyond TM band 4 ($\lambda > 0.9\,\mu$m). Because the generalized curve of dirty ice shows a gradually increasing albedo up to wavelengths of around $1.2\,\mu$m and a high albedo in the infrared, this curve is inconsistent with any of the glacier ice measurements presented here. Most probably this explains why equation (9a) fails to accurately predict the albedo. On the other hand, the generalized curve

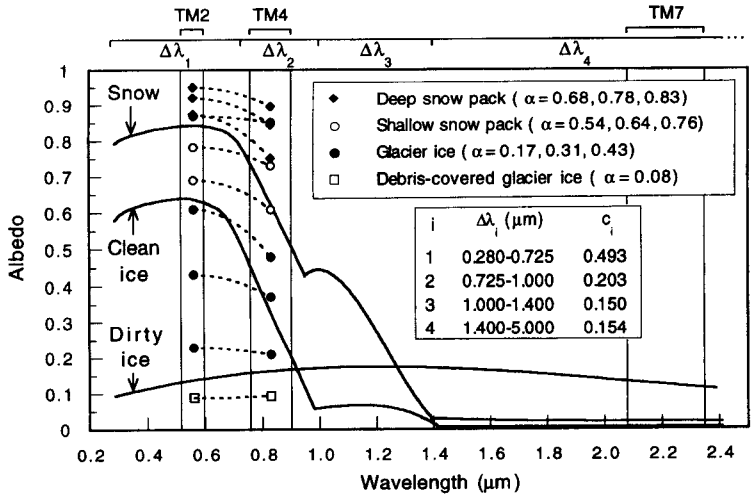

Figure 14. Spectral albedo of glacier ice and snow. The three solid lines are generalized spectral albedo curves of snow, clean ice and dirty ice, presented by Gratton *et al.* (1993) and used by these authors to derive the weighting functions given by equations (9a)–(9c). The symbols $\Delta\lambda_i$ and the coefficients c_i are explained in the text surrounding equations (7) and (8). The data points are characteristic narrowband (TM 2 and 4) measurements carried out on the Morteratschgletscher over deep snow, shallow snow, glacier ice and debris-covered glacier ice. The dotted lines are a guide for the eye. Values of the broadband albedos are given in the legend.

of clean ice does show the typical decrease in the albedo for infrared wavelengths. The curve therefore seems to be consistent with the spectral albedo of the ice surfaces observed on the Morteratschgletscher. This is probably the reason why equation (9b) performs well.

The measurements carried out over snow show that the spectral albedo is diverse (figure 14). In case of deep snow the measurements are in broad agreement with the model calculations of Wiscome and Warren (1980) (figure 12). The visible albedos seem to be rather low compared with the model, but this can be explained by the presence of dust and soot particles. They affect the albedo mainly in the visible where the absorption of light by ice is weakest (Warren and Wiscombe 1981, Warren 1982). The measurements carried out over shallow snow packs suggest that the spectral albedo between 0.5 and 0.9 μm falls off rather slowly. The flatness of the curve is most probably due to the thin snow layer. Since visible radiation penetrates much deeper than near-infrared radiation the underlying ice surface reduces the albedo mainly in the visible and flattens the curve. This has been confirmed earlier by model calculations (Wiscombe and Warren 1980) and observations (Mellor 1977).

Differences in snow grain size and snow pack thickness lead to a great diversity in spectral albedo curves. This complicates the formulation of one weighting function on the basis of the theory presented at the beginning of this section. In fact the assumption that the ratio $\alpha(\Delta\lambda_3)/\alpha_4$ is constant implies *a priori* that the theory is not suitable for constructing a single weighting function for snow packs in different stages of metamorphosis (figure 12). Obviously differences in snow pack thickness limit the usefulness of the theory even more. It is therefore not surprising that the

existing weighting functions in general fail to predict the measurements made over snow.

6. Conclusion

A very important element of the present paper is equation (6). This empirical relationship enables users of Landsat TM data to calculate the broadband albedo of any type of glacier ice or snow observed on the Morteratschgletscher from albedos in TM bands 2 and 4. We feel that the situation on the Morteratschgletscher is typical for Alpine glaciers in general, which means that equation (6) can probably be used in any Landsat-TM based study of the albedo of Alpine glaciers. Needless to say, the correctness of this supposition should be tested with additional narrowband and broadband albedo measurements carried out on other glaciers.

It should be noted that the different terms in equation (6) refer to hemispherical surface reflectances. Therefore one needs to take into account the anisotropy of the reflected radiation field over the glacier surface before applying the relationship to Landsat TM satellite measurements. Effects of the atmosphere between the satellite sensors and the glacier surface need also to be considered, as well as effects related to the surface topography and the surrounding terrain. Knap and Reijmer (1998) discussed the problem of anisotropy on the basis of directional measurements made also on the Morteratschgletscher. This problem and other aspects of surface-albedo retrieval from TM data are discussed by e.g. Winther (1993) and Knap *et al.* (1998).

The albedo measurements that provided the basis for equation (6) were used to verify weighting functions presented in earlier literature (Duguay and LeDrew 1992, Gratton *et al.* 1993, Duguay 1993). Unfortunately large differences between weighted and measured albedo values appeared frequently (figures 13(*a*) and (*b*)). Another problem is that the aforementioned authors designed different functions for different surface types like dirty ice, clean ice and snow with different grain sizes. It is therefore necessary to classify the glacier surface in TM imagery according to the surface type. We feel that classification is problematic because surface types are not easily separated on the basis of an obvious criterion.

The measurements made on the Morteratschgletscher have shown that the diversity of the spectral albedo of glacier ice and snow is too high to be described by one generalized spectral albedo curve. It is therefore very improbable that the approach proposed by Brest and Goward (1987) and Brest (1987) (described in §5.4) will lead to the formulation of a single suitable linear weighting function that is applicable to any arbitrary glacier surface. Although our empirical approach has a less firm physical basis, it has the obvious advantage that it has led to the formulation of a single relationship that allows an accurate calculation of the broadband albedo of many types of glacier surface ranging from completely debris-covered glacier ice to dry snow. Therefore the application of equation (6) makes glacier surface classifications in TM imagery redundant.

Acknowledgements

Financial support for this project was provided by Space Research Organization Netherlands (SRON). We thank all the people from Kipp & Zonen who were involved in the development of the narrowband pyranometers, particularly Leo van Wely. Special thanks are due to Wim Boot, Henk Snellen and Marcel Portanger (Institute for Marine and Atmospheric research Utrecht; IMAU) for technical support. We also thank Fouke Kuik, Frank Helderman and André van Londen

(Royal Netherlands Meteorological Institute) for assistance during calibration of the instruments and for allowing us to make comparative measurements with the optical multichannel analyzer. Bas Henzing is thanked for assistance in the field. Thanks are due to Stephen Warren (University of Washington, Seattle, USA) who provided us with the data for figure 12. We thank the people of the Ice and Climate group of IMAU for providing helpful comments. We are grateful to Sheila McNab for improving the English of the manuscript.

References

ARNOLD, N. S., WILLIS, I. C., SHARP, M. J., RICHARDS, K. S., and LAWSON, W. J., 1996, A distributed surface energy-balance model for a small valley glacier. I. Development and testing for Haut Glacier d'Arolla, Switzerland. *Journal of Glaciology*, **42**(140), 77–89.

BREST, C. L., 1987, Seasonal albedo of an urban/rural landscape from satellite observations. *Journal of Climate and Applied Meteorology*, **26**, 1169–1187.

BREST, C. L., and GOWARD, S. N., 1987, Deriving surface albedo measurements from narrow band satellite data. *International Journal of Remote Sensing*, **8**(3), 351–367.

BROCK, B. W., 1997, Seasonal and spatial variations in the surface energy-balance of valley glaciers. Unpublished Ph.D. Thesis, University of Cambridge, UK.

DUGUAY, C. R., 1993, Modelling the radiation budget of alpine snowfields with remotely sensed data: model formulation and validation. *Annals of Glaciology*, **17**, 288–294.

DUGUAY, C. R., and LEDREW, E. F., 1991, Mapping surface albedo in the east slope of the Colorado Front Range, U.S.A., with Landsat Thematic Mapper. *Arctic and Alpine Research*, **23**, 213–223.

DUGUAY, C. R., and LEDREW, E. F., 1992, Estimating surface reflectance and albedo from Landsat-5 Thematic Mapper over rugged terrain. *Photogrammetric Engineering and Remote Sensing*, **58**(5), 551–558.

GRATTON, D. J., HOWART, P. J., and MARCEAU, D. J., 1993, Using Landsat-5 Thematic Mapper and Digital Elevation Data to determine the net radiation field of a mountain glacier. *Remote Sensing of Environment*, **43**, 315–331.

GRENFELL, T. C., and MULLEN, P. C., 1994, Reflection of solar radiation by the Antarctic snow surface at ultraviolet, visible and near-infrared wavelengths. *Journal of Geophysical Research*, **99**, 18669–18684.

HAEBERLI, W., 1995, Glacier fluctuations and climate change detection—operational elements of a worldwide monitoring strategy. *Bulletin of the World Meteorological Organization*, **44**(1), 23–31.

HALL, D. K., CHANG, A. T. C., and SIDDALINGAIAH, H., 1988, Reflectances of glaciers as calculated using Landsat-5 Thematic Mapper data. *Remote Sensing of Environment*, **25**, 311–321.

IQBAL, M., 1983, *An Introduction to Solar Radiation* (London: Academic Press).

KNAP, W. H., 1997, Satellited-derived and ground-based measurements of the surface albedo of glaciers. Ph.D. thesis, Utrecht University, The Netherlands.

KNAP, W. H., and OERLEMANS, J., 1996, The surface albedo of the Greenland ice sheet: satellite-derived and *in situ* measurements in the Søndre Strømfjord area during the 1991 melt season. *Journal of Glaciology*, **42**, 364–374.

KNAP, W. H., and REIJMER, C. H., 1998, Anisotropy of the reflected radiation field over melting glacier ice: measurements in Landsat-TM bands 2 and 4. *Remote Sensing of Environment*, **65**, 93–104.

KNAP, W. H., BROCK, B. W., OERLEMANS, J., and WILLIS, I. C., 1999, Comparison of Landsat-TM derived and ground-based albedos of Haut Glacier d'Arolla, Switzerland. *International Journal of Remote Sensing* (accepted).

MAISCH, M., BURGA, C. A., and FITZE, P., 1993, *Lebendiges Gletschervorfeld. Führer und Begleitbuch zum Gletscherlehrpfad Morteratsch* (Samedan, Switzerland: Engadin-Press AG).

MARKHAM, B. L., and BARKER, J. L., 1983, *Spectral Characterization of the Landsat Thematic Mapper Sensors*. NASA Conference Publication, 2355, pp. 235–276.

MELLOR, M., 1977, Engineering properties of snow. *Journal of Glaciology*, **1**, 15–66.

OERLEMANS, J., 1993, A model for the surface balance of ice masses: part I. Alpine glaciers. *Zeitschrift für Gletscherkunde und Glazialgeologie*, **27/28**, 63–83.

OERLEMANS, J., 1997, Glacio-meteorological investigations on the Morteratschgletscher, Switzerland. Report no. 1. IMAU report R 97-7. Utrecht University, The Netherlands.

OERLEMANS, J., and KNAP, W. H., 1998, A one-year record of global radiation and albedo in the ablation zone of the Morteratschgletscher, Switzerland. *Journal of Glaciology*, **44**(147), 231–238.

SLINGO, A., and SCHRECKER, H. M., 1982, On the shortwave radiative properties of stratiform water clouds. *Quarterly Journal of the Royal Meteorological Society*, **108**, 407–426.

WARREN, S. G., 1982, Optical properties of snow. *Reviews of Geophysics and Space Physics*, **20**(1), 67–89.

WARREN, S. G., and WISCOMBE, W. J., 1981, A model for the spectral albedo of snow. II: snow containing atmospheric aerosols. *Journal of the Atmospheric Sciences*, **37**, 2734–2745.

WILLIAMS, R. S., and FERRIGNO, J. G., 1995, Satellite image atlas of glaciers of the world. United States Geological Survey Professional Paper 1386-A.E. United States Government Printing Office, Washington, DC.

WINTHER, J.-G., 1993, Landsat TM derived and in situ summer reflectance of glaciers in Svalbard. *Polar Research*, **12**(1), 37–55.

WISCOMBE, W. J., and WARREN, S. G., 1980, A model for the spectral albedo of snow. I: pure snow. *Journal of the Atmospheric Sciences*, **37**, 2712–2733.

ZENG, Q., CAO, C. M., FENG, X., LIANG, F., CHEN, X., and SHENG, W., 1984, Study on spectral reflectance characteristics of snow, ice and water of northwest China. *Scientia Sinica (Series B)*, **27**, 647–656.